Geosci. Model Dev. Discuss., 8, 2497–2528, 2015
www.geosci-model-dev-discuss.net/8/2497/2015/
doi:10.5194/gmdd-8-2497-2015

Geoscientific Model Development Discussions
Open Access

PyXRD v0.6.2: a FOSS program to quantify disordered, layered minerals using multi-specimen X-ray diffraction profile fitting

M. Dumon and E. Van Ranst

Department of Geology and Soil Science (WE13), Ghent University, Krijgslaan 281/S8, 9000 Ghent, Belgium

Received: 27 November 2014 – Accepted: 23 February 2015 – Published: 5 March 2015

Correspondence to: M. Dumon (mathijs.dumon@ugent.be)

Published by Copernicus Publications on behalf of the European Geosciences Union.

Abstract

This paper presents a free and open-source model called PyXRD (short for Python X-ray diffraction) to improve the quantification of complex, poly-phasic mixed-layer phyllosilicate assemblages. The novelty of this model is the ab initio incorporation of the multi-specimen method, making it possible to share phases and (a selection of) their parameters across multiple specimens. By effectively reducing the number of parameters and increasing the number of observations, this approach speeds up the manual refinement process significantly when automated algorithms are used. To check the hypothesis that the multi-specimen set-up can improve automatic parameter refinement, we calculated X-ray diffraction patterns for four theoretical mineral assemblages. These patterns were then used as input for a refinement employing the multi-specimen set-up and one employing the single-pattern set-ups. For all of the assemblages, PyXRD was able to reproduce or approximate the input parameters with the multi-specimen approach. Diverging solutions only occurred in single-pattern set-ups which do not contain enough information (e.g. patterns of heated samples) to discern all the different minerals. Assuming a correct qualitative interpretation was made and a single pattern exists in which all phases are sufficiently discernible, the obtained results indicate a good quantification can often be obtained with just that pattern. For naturally occurring samples, this could mean modelling air-dry and/or ethylene-glycolated patterns might be sufficient. However, these results from theoretical experiments cannot automatically be extrapolated to all real-life experiments. In any case, PyXRD has proven to be very useful when X-ray diffraction patterns are modelled for complex mineral assemblages containing mixed-layer phyllosilicates with a multi-specimen approach.

1 Introduction

Clay minerals (i.e. phyllosilicates) are among the most difficult minerals to study in detail due to their inherent chemical and structural variability (Środoń, 2006; Velde and

GMDD
8, 2497–2528, 2015

Meunier, 2008; Hubert et al., 2012). Nonetheless, these minerals are one of the most abundant constituents of the Earth's upper crust, and have an important influence on various physical (e.g. plasticity, shear strength, porosity) and chemical (e.g. buffering and exchange capacities, pH, electrical conductivity) properties. Phyllosilicates are also very reactive phases responding quickly to changes in their environment (Pai et al., 2004; Meunier, 2007; Velde and Meunier, 2008; Cornelis et al., 2014).

Therefore, quantitative information on the mineralogical composition of clay-bearing samples is an important step in characterizing and understanding them. Different techniques can be used to quantify clay minerals, but those using X-ray diffraction are the most abundant and have proven to be the most reliable (Righi et al., 1999; Środoń, 2006; Hubert et al., 2009, 2012; Ufer et al., 2012a, b). Methods that rely on calculating X-ray diffraction patterns usually provide the highest level of detail because the input for such models can be considered an approximation of the real structure of the minerals (e.g. layer structures, composition, stacking parameters, interlayer composition, orientation). As such, this approach does not only yield quantitative data, but also structural and compositional information. However, this also means a large number of variables are involved, some of which are very difficult to predict or estimate in advance. In combination with the complex, polyphasic nature of many natural samples, it is a challenge to create software that allows for the completely automated quantification of clay minerals.

Nonetheless, in the past few decades several computer programs have been developed to calculate X-ray diffraction patterns for (disordered) clay minerals. Examples are the NEWMOD-family (Pevear and Schuette, 1993; Yuan and Bish, 2010), MLM2C/3C and derivatives (Plançon and Drits, 2000), Sybilla (Aplin et al., 2006) and BGMN (Ufer et al., 2012a, b). Some of these programs (e.g. BGMN, Wildfire, Sybilla 3-D) are able to calculate X-ray diffraction patterns for randomly oriented three-dimensional powder diffraction patterns, while others (NEWMOD, MLM2C, MLM3C, Sybilla) focus only on calculating one-dimensional (00l) patterns. The latter have the advantage of requiring less input (e.g. no parameters are needed to describe the rotational and translational

GMDD
8, 2497–2528, 2015

(dis)order of the layers) and may be easier to use compared to their 3-D counterparts. Yet, they also have drawbacks, as they are unable to model polytypes or quantify unoriented, non-lamellar phases (e.g. quartz, feldspars, etc.) together with the phyllosilicates.

Another aspect to consider is the ability of these models to automatically refine parameters. For instance, the last version of NEWMOD® uses a simple least-squares algorithm, Sybilla© makes use of a genetic algorithm, and BGMN has a custom least-squares algorithm. These algorithms always require some guidance e.g. by not releasing all parameters for automatic refinement at once, by adjusting some parameters manually, by setting upper and lower limits or by having sane starting values, close enough to the actual solution. The reason is that these models are usually poorly constrained, and a successful quantification is still very dependent on the skill of the individual modeller. As a result, most published quantifications of complex mixed-layer assemblages had to employ a time-consuming trial-and-error approach at some point in the modelling process.

Several authors used a "multi-specimen approach" to further constrain their models (Drits, 1997; Sakharov et al., 1999a, b; Meunier, 2005; Lanson, 2011; Hubert et al., 2012). This concept involves recording multiple specimens (e.g. air-dried, glycolated, heat treatments) of the same sample. When these patterns are then used for quantification, the same structural model, aside from some small deviations or changes related to the treatment, should be able to explain the observed patterns equally well. Nevertheless, today not a single model allows for a side-by-side calculation of these patterns. Because of this, modellers are still forced to refine their model on one specimen and then check if the solution also explains the other observations. As long as a manual trial-and-error refinement process is used, this does not pose too many practical problems aside from the time needed. However, a computer model able to integrate all the observations and calculate patterns for them could lead to better automatic parameter refinements.

GMDD
8, 2497–2528, 2015

The computer model presented in this article, called PyXRD (short for Python X-ray Diffraction), was designed with this multi-specimen approach in mind. It (selectively) shares phase parameters across specimens and keeps phase quantities identical in each specimen, thus reducing the number of parameters while at the same time increasing the number of observations. Other design goals for PyXRD were (i) to have an easy-to-use interface, (ii) to be an open model allowing as many aspects of the input to be changed as possible, (iii) to provide a means for automatic parameter refinement, and (iv) to provide an open-source model for others, allowing them to use the software freely and make improvements where they see fit.

This paper illustrates the general structure of this model and presents the results from a comparison between automatic parameter refinements for several theoretical mineral assemblages, with and without the use of the multiple-specimen approach. The software manual contains more detailed information about the numerical solutions used for calculating the X-ray diffraction patterns and a guided example on how to create projects using the graphical user interface (GUI).

2 Materials and methods

2.1 Model implementation and licence

PyXRD is written in Python 2.7 and uses a number of open-source third-party modules. The GUI utilizes PyGTK as widget toolkit and has an internal model-view-controller framework. To improve calculation speed, PyXRD makes use of the NumPy and SciPy libraries. NumPy provides multidimensional array objects and many related routines for manipulating them, while SciPy provides more complex mathematical and scientific algorithms built on top of NumPy (Jones et al., 2001; van der Walt et al., 2011). The Matplotlib library is used for plotting patterns and data (Hunter, 2007). Finally, the Distributed Evolutionary Algorithms for Python (DEAP) library is used to harness to power of evolutionary algorithms to automatically refine parameters (Fortin et al., 2012).

GMDD
8, 2497–2528, 2015

PyXRD is released under a BSD licence, except for the mvc module which, as it is a derived work from the gtkmvc project, is licensed as GNU LGPL v2.

2.2 Model data structure

PyXRD is implemented according to a model-view-controller (mvc) paradigm separating data and calculations from GUI-related aspects. In the following section, an overview is given of the most important objects found in the data layer and their associations. More details can also be found in the manual and the source code documentation.

2.2.1 Project object

The user interface of PyXRD can create (or load) a single *Project* object. It is a container object grouping lists of *AtomType*, *Phase*, *Specimen* and *Mixture* objects together. These are the four top-level objects which are used to calculate X-ray diffraction patterns. Their associations are shown schematically in Fig. 1. The purpose of each of them will be explained in more detail below.

2.2.2 AtomType object

The *AtomType* object is the most basic building block. This object bundles all the physical constants (e.g. charge, atomic weight, scattering factors) for a single ion (e.g. Fe^{2+}, Fe^{3+}) or for a molecule (e.g. H_2O and glycol) small enough to be considered having a spherical electron cloud. When a new project is created, a default list of these *AtomType* objects is loaded, using the atomic scattering factors as published by Waasmaier and Kirfel (1995).

GMDD
8, 2497–2528, 2015

2.2.3 Phase and Component objects

Phase objects contain all the information needed to calculate a one-dimensional X-ray diffraction pattern of a (mixed-layer) mineral. A *Phase* combines (i) a *Probability* object, (ii) an object describing the coherent scattering domain size (CSDS), and (iii) one or more *Component* objects contain information about the structure of the different types of layers in the *Phase*. The *Probability* object describes how these layers are stacked by means of Markovian statistics and the Reichweite concept (Drits and Tchoubar, 1990). The CSDS object describes what type of coherent scattering domain size distribution should be used and contains the necessary parameter values (e.g. average CSDS) (Drits et al., 1997). Two types are currently implemented: a generic log-normal distribution and a log-normal distribution in which the values published in Drits et al. (1997) are employed and the average CSDS is the only remaining unknown variable. Each phase also has a σ^* factor which makes it possible to correct for incomplete preferred orientation (Dohrmann et al., 2009).

A *Component* object describes the size, structure, composition and (variation in) basal spacing of a single layer type in that phase. A *Component* contains two lists that combine an *AtomType* from the project with its (projected) coordinate along the *c*-axis (also known as the *z* coordinate) and the number of projected ions of that type at that coordinate. The first list involves atoms in the silicate lattice, while the other list describes the (variable) interlayer space. With this approach, the silicate structure can be shared between different phases (e.g. AD and EG states), while the interlayer contents may still be different.

2.2.4 Specimen objects

Specimen objects provide all the information regarding the experimental data (the actual measurements, sample size, etc.) and the *Goniometer* set-up (radius, slit sizes, etc.). They do not hold a direct reference to phases, but are linked with them through *Mixture* objects.

GMDD
8, 2497–2528, 2015

2.2.5 Mixture objects

Mixture objects are the starting point for the actual calculations as they link phases and specimens together. In the user interface, a table can be created by adding just as many rows as there are *Phases* and just as many columns as there are *Specimens*. In the column headers, there are slots where the user can select the *Specimen*. Similarly, the user can select the corresponding *Phase* in each cell of the grid. This enables the user to select different states of smectite for an AD and an EG *Specimen* (see Fig. 2 for a screenshot of the GUI), while keeping unaffected *Phases*, (e.g. kaolinites, micas and chlorites) unchanged.

Once a *Mixture* is created in this way, a number of parameters are available for automatic refinement (e.g. weight fractions from the *Probability* object, the average CSDS, etc.). In a refinement dialog, the user can select which parameters s/he would like to improve and the minimum and maximum values between which the ideal value should lie. A number of different refinement methods are also available – some of them more complex or specialized than others. Yet, as a complete description of all methods is beyond the scope of this article, only the algorithm used for the refinements will be explained in detail below.

2.3 Numerical calculations

The X-ray diffraction patterns are calculated using the matrix formalism, as detailed in Drits and Tchoubar (1990). An overview of the numerical calculations, are implemented in the "calculations" module, can also be found in the manual. To improve calculation speed, programs can make use of multi-threading, spreading the load from the different threads evenly over the different cores in a multi-core CPU. However, multi-threading is not very effective in Python because of the Global Interpreter Lock (GIL). This lock can only be obtained by a single active thread, while the others have to wait for it to be released again. So instead of multi-threading, PyXRD uses multi-processing, which creates a new python interpreter for each process, circumventing the GIL problem.

GMDD
8, 2497–2528, 2015

The downside is that processes, unlike threads, do not share memory. Therefore, each process needs to be given all the data required to run the calculation. This is achieved by isolating the calculation functions from objects and by extracting the required data from the objects described in the previous section. As a result, the data exchanged between processes is reduced to a minimum. This approach also makes it possible to run PyXRD refinements effectively on high-performance computing (HPC) clusters. As such, it was also used in the experiments presented in this paper.

2.4 Refinement algorithm

PyXRD supports several refinement algorithms, but for more complex problems involving several parameters, the evolutionary strategies (ESs) are found to be most reliable. PyXRD implements several ESs, among which are a Covariance Matrix Adaptation Evolutionary Strategy (CMA-ES) (Hansen and Ostermeier, 2001) and a (multiple) Particle Swarm Optimization (PSO) (Blackwell et al., 2008). While the PSO is effective at searching a parameter space for minima, being able to escape local minima easily, it can take a lot of function calls for it to converge. On the other hand, CMA-ES is much more effective for local searches, but does get stuck in local minima more easily. Therefore, PyXRD also implements a Particle Swarm CMA-ES (PS-CMA-ES) algorithm which extends the CMA-ES with collaborative concepts from PSO (Muller et al., 2009), making it the more robust choice. This PS-CMA-ES was also used in the experiments presented below.

3 Test case simulations

In total, four theoretical mineral assemblages were tested (Table 1):

Assemblage 1 is a very simple test because of the absence of overlapping and similar phases. Its main purpose was to see whether the model and, more importantly, the selected refinement strategy, can produce a reliable result. The assemblage consists

GMDD
8, 2497–2528, 2015

of equal amounts of a discrete kaolinite, a discrete illite and an R0 illite/smectite with only 10 % illite layers.

Assemblage 2 is more complex, comprising six different phases: a discrete illite, a discrete kaolinite, an R0 illite/smectite with 65 % illite layers, an R0 kaolinite/smectite with 80 % kaolinite layers, a smectite and a poorly-crystalline chlorite. The idea behind this assemblage was to mimic phases encountered in some soils. The poorly-crystalline chlorite component can be interpreted as a small amount of hydroxy-interlayered smectite (or vermiculite) and is not to be considered a primary trioctahedral chlorite, while the kaolinite/smectite represents a neoformed, defective kaolinite or smectite. This kind of phase has been reported a number of times, usually in finer clay fractions (≤ 0.2 µm) of certain soils (Hubert et al., 2009, 2012; Ryan and Huertas, 2009; Dumon et al., 2014). The different phases are also present in different quantities, with the illite-bearing phases each contributing 25.0 wt %, the smectite taking up 20.0 wt %, the kaolinite phases each accounting for 12.5 wt % and the chlorite being a minor phase with only 5.0 wt %.

Assemblage 3 is composed of 30 % discrete illite, 35 % kaolinite, 20 % high-charge smectite (vermiculite-like) and 15 % low-charge smectite. The main idea behind this test assemblage was to see whether the presence of high-charge and low-charge phases (which in this case produced similar patterns under AD and heated conditions, but different patterns under EG conditions) has an influence on the refinement and the quantification in the different set-ups.

Test patterns for assemblage 4 were calculated with 35 % well-crystallized kaolinite (with a high average CSDS), 15 % poorly-crystallized kaolinite (with a low average CSDS) and 50 % of an R0 illite/smectite with 98 % of illite layers. However, these patterns were not modelled in the same structural model. Instead of two different kaolinites, a single kaolinite was added, and instead of an illite/smectite, a discrete illite was used. As such, the influence of simplified model input could be checked, which is common in real-life uses (e.g. due to misinterpretation).

GMDD
8, 2497–2528, 2015

After the necessary phases and their parameters were set up, a calculated pattern was generated from 2 to 50° 2θ with a 0.02° step size, saved and re-imported as experimental data. Random noise was also added to these patterns to approximate real-life data, using the following formula:

$$I_n = I_o \cdot (1 + (X - 0.5) \cdot f_n)$$

where I_n is the intensity with noise, I_o the original intensity, X a random fraction between 0 and 1 and f_n the noise factor, which was set to 0.01. This results in a random deviation of at most 0.5 % above or below the original intensity. For assemblages 1 and 2, both the smooth and noisy patterns were used in separate refinements to assess the influence of this treatment. For assemblages 3 and 4, only the noisy patterns were used, because the previous two experiments showed little influence of the noise on the final results (see below).

Since evolutionary refinement strategies have a stochastic component, each refinement will be different, even if starting and boundary conditions are identical. Nonetheless, the starting point may also have an influence on the final result. To average out these differences and to check if the final output is reproducible, 50 random starting points were sampled so that a normal distribution over the parameter space was obtained. Each of these points was applied to the model before the refinement started. At the end of the refinements, average parameter values and their standard deviations were calculated for these 50 iterations. Additionally, the model kept track of the best solution found until then in each iteration, allowing us to create parameter evolution plots.

GMDD
8, 2497–2528, 2015

4 Results and discussion

4.1 Assemblage 1

An overview of the obtained average parameter values and standard deviations for assemblage 1 can be found in Tables 2 and 3. Parameter evolution plots for two selected parameters (the average CSDS and the fraction of illite layers in the illite/smectite) are also shown in Fig. 3. Most parameters are determined accurately and with very high precision. The difference between noisy patterns and smooth patterns is marginal, and no difference can be observed between the runs where multiple specimens are combined and those where only a single specimen was used for refinement. As a result of this, the obtained weight fractions for the three phases are also very accurate, with only a small (and systematic) deviation for runs using noisy patterns.

These results prove that the PS-CMA-ES refinement strategy implemented in PyXRD is able to produce excellent results. However, the obtained level of accuracy is not a realistic level for natural samples, but stems from the simplicity of this set-up.

4.2 Assemblage 2

An overview of the obtained average parameter values and standard deviations for assemblage 2 can be found in Tables 4 and 5. As was the case in the previous assemblage, no significant difference can be observed between runs that use smooth patterns and those that use noisy ones. Both types produced similar parameter accuracies and precisions. Overall, the results are less accurate and precise compared to assemblage 1, but still very good. Most notably, the weight fractions of the smectite layer types in the kaolinite/smectite show a much larger imprecision. This is also the case in the parameter evolution plots (Fig. 4) for these fractions. An explanation can be found in the sensitivity of these parameters: since the kaolinite fraction in this mixed-layer is relatively high (80 %), the relative amounts of the different types of smectite do

GMDD
8, 2497–2528, 2015

not have such a large influence on the calculated pattern. Most likely, the refinement strategy was not given enough time to fully converge for these insensitive parameters.

Some differences are also noticeable between runs that combine multiple specimens and those where only heated patterns were used. For the latter, the imprecision on the weight fractions for the illite, illite/smectite and smectite phases is significantly larger compared to the other runs. This is to be expected, as heating collapses swelling layers, causing significant peak overlap with the illite peaks. Despite this overlap, it was still possible to obtain accurate and precise averages for the other parameters, comparable to the other runs.

4.3 Assemblage 3

An overview of the obtained average parameter values and standard deviations for assemblage 3 can be found in Table 6. With this assemblage, the combined set-up and the set-up using only the EG pattern both resulted in the same performance, giving accurate and precise parameter values. The set-up with AD or heated patterns, on the other hand, led to inaccurate and imprecise results, especially when the weight fractions are taken into account. Finally, it can also be observed that the weight fractions and parameter values of phases that were unaffected by the treatments (i.e. kaolinite and illite) are more accurate and precise in these set-ups. It is mainly for the overlapping phases (i.e. smectites) that the errors occur.

Figure 5 shows the parameter plots for the multi-specimen set-up and the AD set-up for a few selected parameters. This figure illustrates the divergent nature of some parameters in the AD set-up very well, while it is clear that the combined set-up does not suffer from this as it has access to the EG pattern as well.

The outcome of this experiment is in line with our expectations, as only the EG pattern contains enough information to distinguish these two smectites from each other. When the EG pattern is absent, the results become divergent, resulting in the high imprecision observed for the AD and heated pattern set-ups.

GMDD
8, 2497–2528, 2015

4.4 Assemblage 4

An overview of the obtained average parameter values and standard deviations for assemblage 4 can be found in Table 7. In this set-up, we intentionally misidentified a mixed-layer illite/smectite as an illite and overlooked the presence of two populations of kaolinite instead of one. Nevertheless the model is able to give us decent parameter accuracies. These kinds of "mistakes" are quite common in the real-life use of this model, and apparently do not matter too much either, as long as they are related to natural inhomogeneities. In contrast, a model based on a completely wrong interpretation will never yield any good output, and will result in a very obvious mismatch between the calculated and observed patterns. Even in this assemblage, the (residual) XRD patterns (Fig. 6) show a clear mismatch for these phases. An observant user should notice this and as such be able to identify wrong and/or missing phases.

4.5 Summary

For all four assemblages, PyXRD has been able to reproduce the input parameters or at least approximate them with the multi-specimen approach. The only complications occur when single patterns are used which do not contain enough information on their own (e.g. in most cases heated patterns).

These theoretical experiments seem to suggest that the multiple-specimen approach does not add a lot of constraints to the mathematical model, although it can help uncover flawed interpretations. Instead, it appears far more important to correctly identify the phases using multiple specimens than to use these for the parameter refinement. Once the phases are identified, a good quantification can often be obtained with only a single pattern if all phases can be sufficiently discerned from one another in that state. For most natural samples, this could imply that it is sufficient to model the EG and/or the AD pattern. Indeed, only AD and/or EG patterns are used in many papers presenting modelled X-ray diffraction patterns of phyllosilicates (Plançon and Roux, 2010; Hubert et al., 2012; Ufer et al., 2012a; Dumon et al., 2014). However, it is impor-

GMDD
8, 2497–2528, 2015

tant to realize that these results from theoretical experiments cannot automatically be extrapolated to all real-life modelling experiments.

In this context, one can also wonder how realistic it is to share some of the parameters between the different specimens during the refinement. Some of them are rather difficult to control from experiment to experiment. For example, the number of water or glycol layers intercalated into smectite bearing phases is not only dependent on layer charge and the saturating cation, but also on the ambient conditions (i.e. temperature and relative humidity) (Tamura et al., 2000). If, because of this, a lot of the parameters cannot be shared, the advantage of having added more observations is quickly lost by having to add more parameters.

5 Conclusion

In this paper we have presented PyXRD, a new, free and open-source program to perform a (semi-)quantitative analysis of disordered layered minerals using multi-specimen X-ray diffraction profile fitting. It is the authors' sincere hope that others will pick up on the model and improve it. The novelty of this model lies specifically in the ab initio incorporation of the multi-specimen method, making it possile to share phases and (a selection of) their parameters across multiple specimens. In theory, this should constrain the mathematical model better and improve the automatic parameter refinement results (Sakharov et al., 1999a; Meunier, 2005; Lanson, 2011). Nevertheless, although the possibility to model several specimens at once is an important step forward, results from theoretical experiments indicate that the multiple specimen method is not always required to obtain good parameter estimates. Rather, it is more important to have a good identification of the phases present, for which the multiple-specimen approach is definitely helpful. We can conclude that PyXRD has proven to be very useful when X-ray diffraction patterns for complex mineral assemblages containing (mixed-layer) phyllosilicates are modelled with a multi-specimen approach.

GMDD
8, 2497–2528, 2015

Code availability

The source code for PyXRD can be found online at https://github.com/mathijs-dumon/PyXRD, together with installation instructions and a manual with detailed information regarding the calculations and a step-by-step example on how to use the user interface.

The Supplement related to this article is available online at doi:10.5194/gmdd-8-2497-2015-supplement.

Acknowledgements. This research was funded by the project G028714N of the Fund for Scientific Research (Flanders). The computational resources (Stevin Supercomputer Infrastructure) and services used in this work were provided by the VSC (Flemish Supercomputer Center), funded by Ghent University, the Hercules Foundation and the Flemish Government (Department EWI), for which we are very grateful.

References

Aplin, A. C., Matenaar, I. F., McCarty, D. K., and van der Pluijm, B. A.: Influence of mechanical compaction and clay mineral diagenesis on the microfabric and pore-scale properties of deep-water Gulf of Mexico mudstones, Clay. Clay Miner., 54, 500–514, 2006.

Blackwell, T., Branke, J., and Li, X.: Particle swarms for dynamic optimization problems, in: Swarm Intelligence, edited by: Blum, C. and Merkle, D., Natural Computing Series, Springer, Berlin, Heidelberg, 193–217, 2008.

Cornelis, J.-T., Weis, D., Lavkulich, L., Vermeire, M.-L., Delvaux, B., and Barling, J.: Silicon isotopes record dissolution and re-precipitation of pedogenic clay minerals in a podzolic soil chronosequence, Geoderma, 235–236, 19–29, 2014.

Dohrmann, R., Rüping, K. B., Kleber, M., Ufer, K., and Jahn, R.: Variation of preferred orientation in oriented clay mounts as a result of sample preparation and composition, Clay. Clay Miner., 57, 686–694, 2009.

GMDD
8, 2497–2528, 2015

Drits, V., Środoń, J., and Eberl, D. D.: XRD Measurement of mean crystallite thickness of illite and illite/smectite: reappraisal of the Kubler Index and the Scherrer Equation, Clay. Clay Miner., 45, 461–475, 1997.
Drits, V. A.: Mixed-layer minerals, in: Modular Aspects of Minerals, edited by: Merlino, S., EMU Notes in Mineralogy, Eötvös University Press, Budapest, 153–190, 1997.
Drits, V. A. and Tchoubar, C.: X-Ray Diffraction by Disordered Lamellar Structures: Theory and Applications to Microdivided Silicates and Carbons, Springer-Verlag, Berlin, Germany, 1990.
Dumon, M., Tolossa, A. R., Capon, B., Detavernier, C., and Van Ranst, E.: Quantitative clay mineralogy of a Vertic Planosol in southwestern Ethiopia: impact on soil formation hypotheses, Geoderma, 214–215, 184–196, 2014.
Fortin, F.-A., De Rainville, F.-M., Gardner, M.-A., Parizeau, M., and Gagné, C.: DEAP: evolutionary algorithms made easy, JMLR, 13, 2171–2175, 2012.
Hansen, N. and Ostermeier, A.: Completely derandomized self-adaptation in evolution strategies, Evol. Comput., 9, 159–195, 2001.
Hubert, F., Caner, L., Meunier, A., and Lanson, B.: Advances in characterization of soil clay mineralogy using X-ray diffraction: from decomposition to profile fitting, Eur. J. Soil Sci., 60, 1093–1105, 2009.
Hubert, F., Caner, L., Meunier, A., and Ferrage, E.: Unraveling complex < 2 µm clay mineralogy from soils using X-ray diffraction profile modeling on particle-size sub-fractions: implications for soil pedogenesis and reactivity, Am. Mineral., 97, 384–398, 2012.
Hunter, J. D.: Matplotlib: a 2-D graphics environment, Comput. Sci. Eng., 9, 90–95, 2007.
Jones, E., Oliphant, E., Peterson, P., et al.: SciPy: Open Source Scientific Tools for Python, available at: http://www.scipy.org/ (last access: 4 March 2015), 2001.
Lanson, B.: Modelling of X-ray diffraction profiles: investigation of defective lamellar structure crystal chemistry, in: Layered Mineral Structures and Their Application in Advanced Technologies, edited by: Brigatti, M. F. and Mottana, A., EMU Notes in Mineralogy, 151–202, 2011.
Meunier, A.: Clays, Springer, Berlin, Germany, 2005.
Meunier, A.: Soil hydroxy-interlayerd minerals: a re-interpretation of their crystallochemical properties, Clay. Clay Miner., 55, 380–388, 2007.
Muller, C. L., Baumgartner, B., and Sbalzarini, I.: Particle swarm CMA evolution strategy for the optimization of multi-funnel landscapes, in: IEEE Congress on Evolutionary Computation 2009, 2685–2692, 2009.

GMDD
8, 2497–2528, 2015

Pai, C. W., Wang, M. K., King, H. B., Chiu, C. Y., and Hwong, J.-L.: Hydroxy-interlayered minerals of forest soils in A-Li Mountain, Taiwan, Geoderma, 123, 245–255, 2004.
Pevear, D. R. and Schuette, J. F.: Inverting the NEWMOD(c) X-ray diffraction forward model for clay minerals using genetic algorithms, in: Computer Applications to X-ray Powder Diffraction Analysis of Clay Minerals, Vol. 5, Clay Minerals Society, Boulder, CO, 19–42, 1993.
Plançon, A.: Order-disorder in clay mineral structures, Clay Miner., 36, 1–14, 2001.
Plançon, A. and Drits, V. A.: Phase analysis of clays using an expert system and alculation programs for X-ray difraction by two- and three-component mixed layer minerals, Clay. Clay Miner., 48, 57–62, 2000.
Plançon, A. and Roux, J.: Software for the assisted determination of the structural parameters of mixed-layer phyllosilicates, Eur. J. Mineral., 22, 733–740, 2010.
Righi, D., Terribile, F., and Petit, S.: Pedogenic formation of kaolinite-smectite mixed layers in a soil toposequence developed from basaltic parent material in Sardinia (Italy), Clay. Clay Miner., 47, 505–514, 1999.
Ryan, P. C. and Huertas, F. J.: The temporal evolution of pedogenic Fe–smectite to Fe–kaolin via interstratified kaolin–smectite in a moist tropical soil chronosequence, Geoderma, 151, 1–15, 2009.
Sakharov, B. A., Lindgreen, H., Salyn, A., and Drits, V. A.: Determination of illite-smectite structures using multispecimen X-ray diffraction profile fitting, Clay. Clay Miner., 47, 555–566, 1999a.
Sakharov, B. A., Lindgreen, H., Salyn, A. L., and Drits, V. A.: Mixed-layer kaolinite-illite-vermiculite in North Sea shales, Clay Miner., 34, 333–344, 1999b.
Środoń, J.: Identification and quantitative analysis of clay minerals, in: Handbook of Clay Science, Developments in Clay Science, Elsevier, USA, 765–787, 2006.
Tamura, K., Yamada, H., and Nakazawa, H.: Stepwise hydration of high-quality synthetic smectite with various cations, Clay. Clay Miner., 48, 400–404, 2000.
Ufer, K., Kleeberg, R., Bergmann, J., and Dohrmann, R.: Rietveld refinement of disordered illite-smectite mixed-layer structures by a recursive algorithm. Part 1: One-dimensional patterns, Clay. Clay Miner., 60, 507–534, 2012a.
Ufer, K., Kleeberg, R., Bergmann, J., and Dohrmann, R.: Rietveld refinement of disordered illite-smectite mixed-layer structures by a recursive algorithm. Part 2: Powder-pattern refinement and quantitative phase analysis, Clay. Clay Miner., 60, 535–552, 2012b.

GMDD
8, 2497–2528, 2015

Van der Walt, S., Colbert, S. C., and Varoquaux, G: The NumPy array: a structure for efficient numerical computation, Comput. Sci. Eng., 13, 22–30, 2011.

Velde, B. B. and Meunier, A.: The Origin of Clay Minerals in Soils and Weathered Rocks, Springer-Verlag, Berlin, Germany, 2008.

Waasmaier, D. and Kirfel, A.: New analytical scattering-factor functions for free atoms and ions, Acta Crystallogr. A, 51, 416–431, 1995.

Yuan, H. and Bish, D. L.: NEWMOD+, a new version of the NEWMOD program for interpreting X-ray powder diffraction patterns from interstratified clay minerals, Clay. Clay Miner., 58, 318–326, 2010.

GMDD

8, 2497–2528, 2015

Table 1. Overview of the different test assemblages and the type of pattern that was refined.

	Assemblage	Smooth pattern?	Noisy pattern?
1	33.3 % Kaolinite 33.3 % Illite 33.3 % Illite/Smectite (10/90) R0	yes	yes
2	25.0 % Illite 25.0 % Illite/Smectite (65/35) R0 20.0 % Smectite 12.5 % Kaolinite 12.5 % Kaolinite/Smectite (80/20) R0 5.0 % Chlorite	yes	yes
3	35.0 % Kaolinite 30.0 % Illite 15.0 % High-charge smectite 20.0 % Low-charge smectite	no	yes
4	35.0 % Kaolinite (CSDS = 20) 15.0 % Kaolinite (CSDS = 6) 50.0 % Illite/Smectite (98/2) R0	no	yes

GMDD
8, 2497–2528, 2015

Table 2. Overview of the means and standard deviations for weight fractions and refined parameters for assemblage 1 using smooth patterns.

Assemblage #1 – smooth patterns					Multiple specimens ($n = 50$)	Only AD ($n = 50$)	Only EG ($n = 50$)	Only 350 heated ($n = 50$)
Phase	Property name	True value	Range Min.	Range Max.	Obtained value $\mu \pm \sigma$	Obtained value $\mu \pm \sigma$	Obtained value $\mu \pm \sigma$	Obtained value $\mu \pm \sigma$
Kaolinite	wt %	33.3	–	–	33.3 ± 0.00	33.3 ± 0.00	33.3 ± 0.00	33.3 ± 0.00
	T	10.0	8.0	20.0	10.0 ± 0.00	10.0 ± 0.00	10.0 ± 0.00	10.0 ± 0.00
Illite	wt %	33.3	–	–	33.3 ± 0.00	33.3 ± 0.00	33.3 ± 0.00	33.3 ± 0.00
	T	10.0	8.0	20.0	10.0 ± 0.00	10.0 ± 0.00	10.0 ± 0.00	10.0 ± 0.00
Illite/Smectite R0	wt %	33.3	–	–	33.3 ± 0.00	33.3 ± 0.00	33.3 ± 0.00	33.3 ± 0.00
	T	5.0	3.0	10.0	5.0 ± 0.00	5.0 ± 0.00	5.0 ± 0.00	5.0 ± 0.00
	Illite content	0.1	0.0	1.0	0.10 ± 0.00	0.10 ± 0.00	0.10 ± 0.00	0.10 ± 0.00
	2wat/(2wat + 1wat)	0.5	0.0	1.0	0.50 ± 0.00	0.50 ± 0.00	–	–
	2gly/(2gly + 1gly)	0.5	0.0	1.0	0.50 ± 0.00	–	0.50 ± 0.00	–
	0gly/(0gly + 1gly)	1.0	.0	1.0	1.00 ± 0.00	–	–	1.00 ± 0.00

GMDD
8, 2497–2528, 2015

Table 3. Overview of the means and standard deviations of weight fractions and refined parameters for assemblage 1 using noisy patterns.

Assemblage #1 – Noisy patterns					Multiple specimens ($n = 50$)	Only AD ($n = 50$)	Only EG ($n = 50$)	Only 350 °C ($n = 50$)
Phase	Property name	True value	Range Min.	Max.	Obtained value $\mu \pm \sigma$	Obtained value $\mu \pm \sigma$	Obtained value $\mu \pm \sigma$	Obtained value $\mu \pm \sigma$
Kaolinite	wt %	33.3	–	–	33.4 ± 0.0	33.4 ± 0.0	33.4 ± 0.0	33.4 ± 0.0
	T	10.0	8.0	20.0	10.0 ± 0.0	10.0 ± 0.0	10.0 ± 0.0	10.1 ± 0.0
Illite	wt %	33.3	–	–	33.4 ± 0.0	33.4 ± 0.0	33.3 ± 0.0	33.5 ± 0.0
	T	10.0	8.0	20.0	10.0 ± 0.0	10.0 ± 0.0	10.1 ± 0.0	10.0 ± 0.0
Illite/Smectite R0	wt %	33.3	–	–	33.2 ± 0.0	33.2 ± 0.0	33.2 ± 0.0	33.1 ± 0.0
	T	5.0	3.0	10.0	5.0 ± 0.0	4.9 ± 0.0	5.0 ± 0.0	5.0 ± 0.0
	Illite content	0.1	0.0	1.0	0.10 ± 0.00	0.09 ± 0.00	0.10 ± 0.00	0.10 ± 0.00
	2wat/(2wat + 1wat)	0.5	0.0	1.0	0.50 ± 0.00	0.49 ± 0.00	–	–
	2gly/(2gly + 1gly)	0.5	0.0	1.0	0.50 ± 0.00	–	0.50 ± 0.00	–
	0gly/(0gly + 1gly)	1.0	0.0	1.0	1.00 ± 0.00	–	–	1.00 ± 0.00

GMDD
8, 2497–2528, 2015

Table 4. Overview of the means and standard deviations of weight fractions and refined parameters for assemblage 2 using smooth patterns.

Assemblage #2 – Smooth patterns					Multiple specimens ($n = 50$)	Only AD ($n = 50$)	Only EG ($n = 50$)	Only 350 °C ($n = 50$)
Phase	Property name	True value	Range Min.	Max.	Obtained value $\mu \pm \sigma$	Obtained value $\mu \pm \sigma$	Obtained value $\mu \pm \sigma$	Obtained value $\mu \pm \sigma$
Illite	wt %	25.0	–	–	25.0 ± 0.1	25.0 ± 0.1	25.0 ± 0.0	25.4 ± 0.71
	T	13.0	10.0	30.0	13.0 ± 0.1	13.0 ± 0.0	13.0 ± 0.0	12.9 ± 0.2
Illite/Smectite R0	wt %	25.0	–	–	24.9 ± 0.2	25.0 ± 0.1	25.0 ± 0.0	24.8 ± 0.3
	T	5.0	3.0	10.0	5.1 ± 0.1	5.0 ± 0.0	5.0 ± 0.0	5.0 ± 0.1
	Illite content	0.65	0.5	1.0	0.65 ± 0.00	0.65 ± 0.00	0.65 ± 0.00	0.64 ± 0.03
	2wat/(2wat + 1wat)	0.7	0.0	1.0	0.70 ± 0.01	0.70 ± 0.00	–	–
	2gly/(2gly + 1gly)	0.7	0.0	1.0	0.71 ± 0.02	–	0.70 ± 0.00	–
	0gly/(0gly + 1gly)	1.0	0.8	1.0	0.96 ± 0.03	–	–	0.99 ± 0.01
Kaolinite	wt %	12.5	–	–	12.5 ± 0.0	12.5 ± 0.0	12.5 ± 0.0	12.5 ± 0.0
	T	20.0	10.0	30.0	20.1 ± 0.1	20.0 ± 0.0	20.0 ± 0.0	20.1 ± 0.1
Kaolinite/Smectite R0	wt %	12.5	–	–	12.7 ± 0.2	12.5 ± 0.1	12.5 ± 0.0	12.9 ± 0.2
	T	3.0	3.0	10.0	3.0 ± 0.0	3.0 ± 0.0	3.0 ± 0.0	3.0 ± 0.0
	Kaolinite content	0.80	0.7	1.0	0.80 ± 0.01	0.80 ± 0.00	0.80 ± 0.00	0.79 ± 0.00
	2wat/(2wat + 1wat)	0.25	0.0	0.6	0.26 ± 0.11	0.25 ± 0.02	–	–
	2gly/(2gly + 1gly)	0.50	0.0	0.6	0.44 ± 0.10	–	0.50 ± 0.01	–
	0gly/(0gly + 1gly)	1.00	0.8	1.0	0.93 ± 0.05	–	–	0.93 ± 0.04
Smectite	wt %	20.0	–	–	19.9 ± 0.1	20.0 ± 0.1	20.0 ± 0.0	19.6 ± 0.7
	T	3.0	3.0	10.0	3.0 ± 0.0	3.0 ± 0.0	3.0 ± 0.0	3.0 ± 0.0
	2wat/(2wat + 1wat)	0.60	0.5	1.0	0.60 ± 0.00	0.60 ± 0.00	–	–
	2gly/(2gly + 1gly)	0.90	0.5	1.0	0.90 ± 0.00	–	0.90 ± 0.00	–
	0gly/(0gly + 1gly)	0.90	0.8	1.0	0.92 ± 0.01	–	–	0.90 ± 0.01
Chlorite	wt %	5.0	–	–	5.0 ± 0.0	5.0 ± 0.1	5.0 ± 0.0	5.0 ± 0.0
	T	5.0	3	10	5.0 ± 0.0	5.0 ± 0.0	5.0 ± 0.0	5.0 ± 0.0
	$\partial d_{001} \times 10^3$	5.0	1.0	10.0	5.0 ± 0.1	5.0 ± 0.1	5.0 ± 0.0	5.1 ± 0.1

GMDD
8, 2497–2528, 2015

Table 5. Overview of the means and standard deviations of weight fractions and refined parameters for assemblage 2 using noisy patterns.

Assemblage #2 – Noisy patterns					Multiple specimens ($n = 50$)	Only AD ($n = 50$)	Only EG ($n = 50$)	Only 350 °C ($n = 50$)
Phase	Property name	True value	Range Min.	Max.	Obtained value $\mu \pm \sigma$	Obtained value $\mu \pm \sigma$	Obtained value $\mu \pm \sigma$	Obtained value $\mu \pm \sigma$
Illite	wt %	25.0	–	–	25.1 ± 0.2	25.2 ± 0.1	25.3 ± 0.1	24.8 ± 1.5
	T	13.0	10.0	30.0	13.1 ± 0.1	13.2 ± 0.0	12.9 ± 0.0	13.2 ± 0.3
Illite/Smectite R0	wt %	25.0	–	–	24.6 ± 0.4	25.8 ± 0.2	24.7 ± 0.1	25.8 ± 1.9
	T	5.0	3.0	10.0	5.0 ± 0.1	5.2 ± 0.0	4.9 ± 0.0	5.0 ± 0.4
	Illite content	0.65	0.5	1.0	0.64 ± 0.01	0.65 ± 0.00	0.65 ± 0.00	0.64 ± 0.04
	2wat/(2wat + 1wat)	0.7	0.0	1.0	0.67 ± 0.02	0.70 ± 0.01	–	–
	2gly/(2gly + 1gly)	0.7	0.0	1.0	0.68 ± 0.01	–	0.67 ± 0.00	–
	0gly/(0gly + 1gly)	1.0	0.8	1.0	0.96 ± 0.02	–	–	0.96 ± 0.03
Kaolinite	wt %	12.5	–	–	12.5 ± 0.0	12.3 ± 0.0	12.5 ± 0.0	12.6 ± 0.1
	T	20.0	10.0	30.0	20.1 ± 0.1	20.1 ± 0.0	20.1 ± 0.0	20.0 ± 0.0
Kaolinite/Smectite R0	wt %	12.5	–	–	12.8 ± 0.4	12.1 ± 0.2	12.4 ± 0.1	12.5 ± 0.1
	T	3.0	3.0	10.0	3.0 ± 0.0	3.0 ± 0.0	3.0 ± 0.0	3.0 ± 0.0
	Kaolinite content	0.80	0.7	1.0	0.80 ± 0.01	0.81 ± 0.01	0.81 ± 0.00	0.82 ± 0.00
	2wat/(2wat + 1wat)	0.25	0.0	0.6	0.30 ± 0.11	0.34 ± 0.03	–	–
	2gly/(2gly + 1gly)	0.50	0.0	0.6	0.47 ± 0.10	–	0.54 ± 0.02	–
	0gly/(0gly + 1gly)	1.00	0.8	1.0	0.91 ± 0.05	–	–	0.94 ± 0.04
Smectite	wt %	20.0	–	–	20.1 ± 0.2	19.6 ± 0.2	20.2 ± 0.1	19.5 ± 3.4
	T	3.0	3.0	10.0	3.0 ± 0.0	3.0 ± 0.0	3.0 ± 0.0	3.0 ± 0.2
	2wat/(2wat + 1wat)	0.60	0.5	1.0	0.60 ± 0.01	0.60 ± 0.00	–	–
	2gly/(2gly + 1gly)	0.90	0.5	1.0	0.90 ± 0.01	–	0.90 ± 0.00	–
	0gly/(0gly + 1gly)	0.90	0.8	1.0	0.92 ± 0.01	–	–	0.91 ± 0.02
Chlorite	wt %	5.0	–	–	5.0 ± 0.0	5.1 ± 0.1	4.9 ± 0.0	4.9 ± 0.1
	T	5.0	3	10	5.1 ± 0.0	5.2 ± 0.1	5.2 ± 0.0	5.0 ± 0.0
	$\partial d_{001} \times 10^3$	5.0	1.0	10.0	5.2 ± 0.3	5.5 ± 0.3	4.5 ± 0.2	5.4 ± 0.3

GMDD
8, 2497–2528, 2015

Table 6. Overview of the means and standard deviations of weight fractions and refined parameters for assemblage 3.

Assemblage #3 – Noisy patterns					Multiple specimens ($n = 50$)	Only AD ($n = 50$)	Only EG ($n = 50$)	Only 350 °C ($n = 50$)
Phase	Property name	True value	Range Min.	Max.	Obtained value $\mu \pm \sigma$	Obtained value $\mu \pm \sigma$	Obtained value $\mu \pm \sigma$	Obtained value $\mu \pm \sigma$
Kaolinite	wt %	35.0	–	–	35.0 ± 0.0	35.3 ± 0.6	34.7 ± 0.0	34.9 ± 0.0
	T	18.0	5	40	18.0 ± 0.0	18.0 ± 0.2	18.0 ± 0.0	18.0 ± 0.0
Illite	wt %	30.0	–	–	30.0 ± 0.0	30.0 ± 0.8	30.1 ± 0.1	29.0 ± 0.1
	T	25.0	5	40	25.0 ± 0.0	25.5 ± 0.1	24.8 ± 0.0	25.2 ± 0.12
High-charge smectite	wt %	15.0	–	–	15.1 ± 0.0	16.9 ± 5.9	15.8 ± 0.1	16.0 ± 0.1
	T	10.0	5	40	10.0 ± 0.0	11.3 ± 5.2	10.0 ± 0.0	10.0 ± 0.1
	HC/(HC + LC)	0.90	0.50	1.00	0.90 ± 0.00	0.87 ± 0.06	0.90 ± 0.00	–
Low-charge smectite	wt %	20.0	–	–	19.9 ± 0.0	17.8 ± 7.2	19.4 ± 0.2	20.3 ± 0.2
	T	10.0	5	40	10.0 ± 0.0	12.2 ± 7.4	10.0 ± 0.0	10.2 ± 0.1
	LC/(LC + HC)	0.80	0.50	1.00	0.80 ± 0.00	0.83 ± 0.06	0.80 ± 0.00	–

GMDD
8, 2497–2528, 2015

Table 7. Overview of the means and standard deviations of weight fractions and refined parameters for assemblage 4.

Assemblage #4 – Noisy patterns					Multiple specimens ($n = 50$)	Only AD ($n = 50$)	Only EG ($n = 50$)	Only 350 °C ($n = 50$)
Phase	Property name	True value	Range Min.	Max.	Obtained value $\mu \pm \sigma$	Obtained value $\mu \pm \sigma$	Obtained value $\mu \pm \sigma$	Obtained value $\mu \pm \sigma$
Kaolinite	wt %	50.0	–	–	49.7 ± 0.1	49.3 ± 0.0	50.3 ± 0.2	49.3 ± 0.1
	T	15.8	5	40	15.2 ± 0.1	15.2 ± 0.0	15.2 ± 0.0	15.6 ± 0.0
Illite	wt %	50.0	–	–	50.3 ± 0.1	50.7 ± 0.0	49.7 ± 0.2	50.7 ± 0.1
	T	30.0	5	40	21.2 ± 0.0	18.8 ± 0.0	22.7 ± 0.1	28.0 ± 0.0
	Oct. Fe^{3+}/Oct. Al^{3+}	0.125	0	0.5	0.133 ± 0.000	0.126 ± 0.002	0.151 ± 0.001	0.139 ± 0.001
	K content	1.50	0	2	1.52 ± 0.01	1.49 ± 0.00	1.52 ± 0.01	1.44 ± 0.00

GMDD
8, 2497–2528, 2015

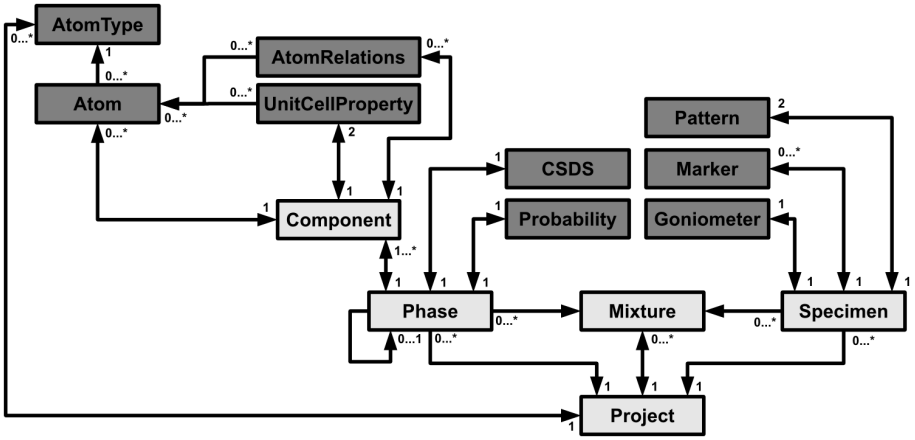

Figure 1. Schematic overview of the most important objects in PyXRD and their relations. Arrows indicate "is referenced *x* times by" relations and the numbers indicate the multiplicity of that relation (e.g. project holds 0 or more references to AtomType).

GMDD
8, 2497–2528, 2015

PyXRD v0.6.2

M. Dumon and
E. Van Ranst

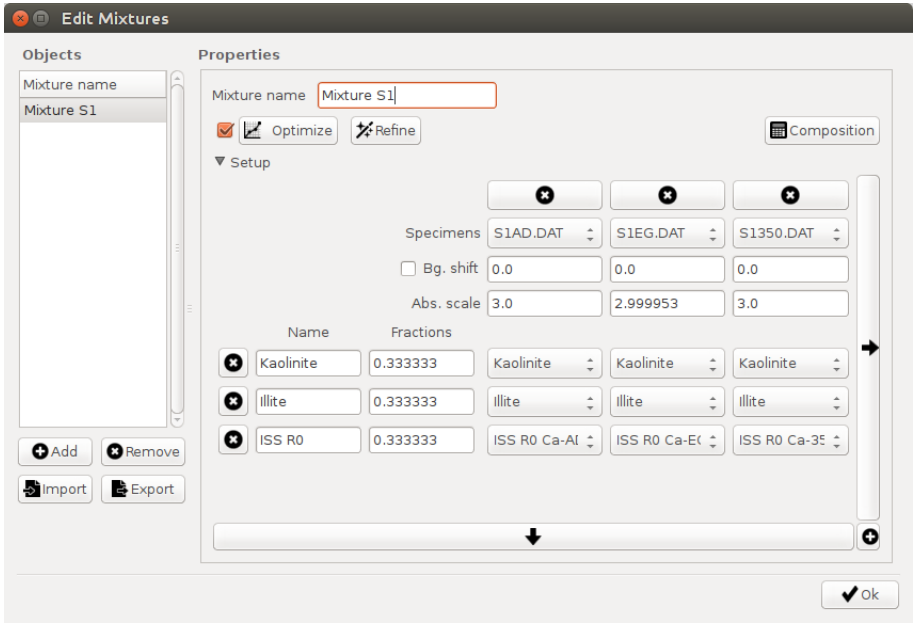

Figure 2. Screenshot showing the "Edit mixtures" dialog where a user can link different phases (Kaolinite, Illite, ISS R0 Ca-AD, . . .) with the corresponding specimens (S1AD.dat, S1EG.dat, . . .).

GMDD
8, 2497–2528, 2015

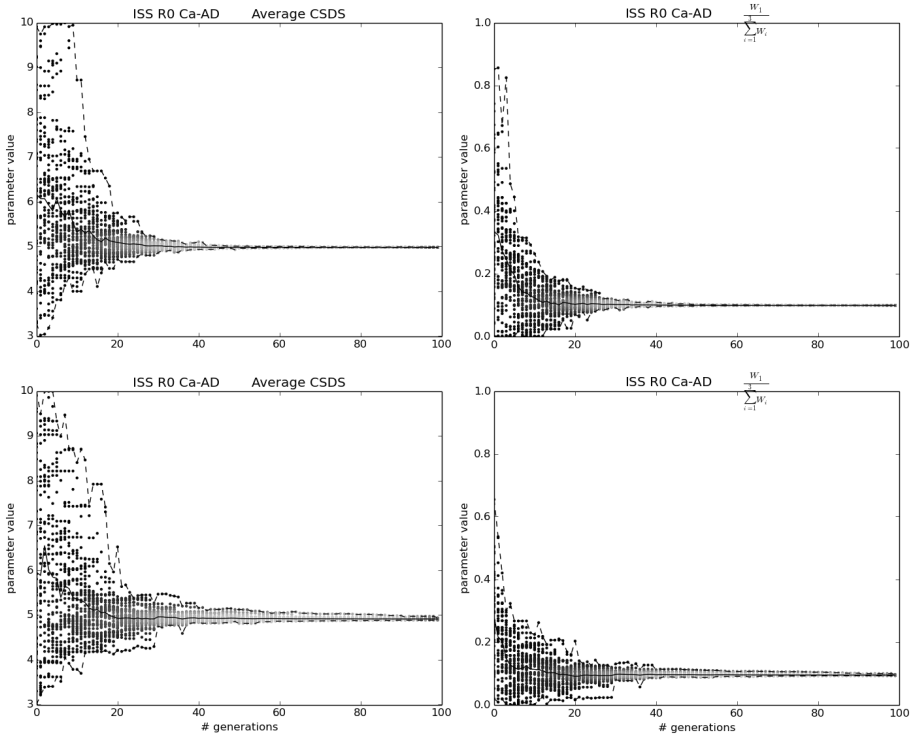

Figure 3. Parameter evolution plots (left: average CSDS; right: illite content) for the noisy patterns of assemblage 1 for the multi-specimen run (top plots) and the isolated AD run (bottom plots). Minimum and maximum values during the refinement are indicated with dashed lines, iterations' best solutions at each generation indicated by dots and average solution with a solid line. The higher the density of the dots, the lighter they are colored.

GMDD
8, 2497–2528, 2015

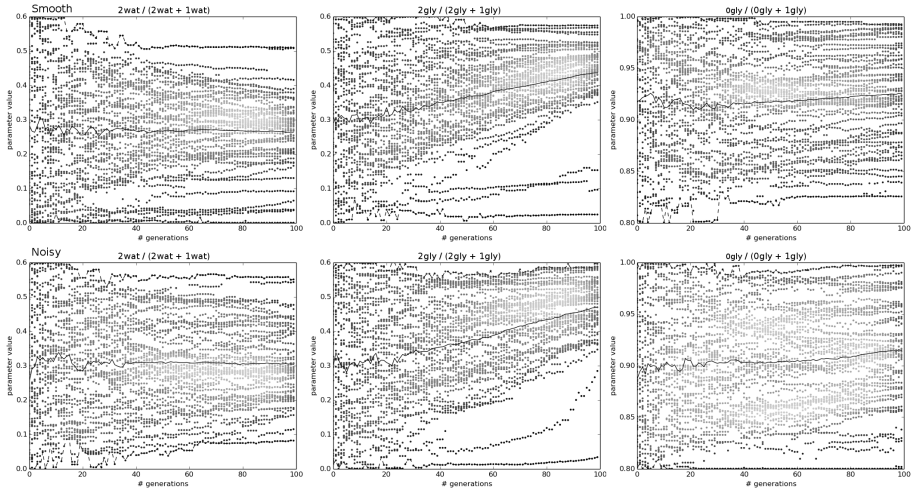

Figure 4. Parameter evolution plots for the smectite fractions in the kaolinite-smectite mixed layer of assemblage 2 using the multi-specimen setup. Plots for the smooth patterns are in the top row, for noisy patterns in the bottom row. Legend as in Fig. 3.

GMDD
8, 2497–2528, 2015

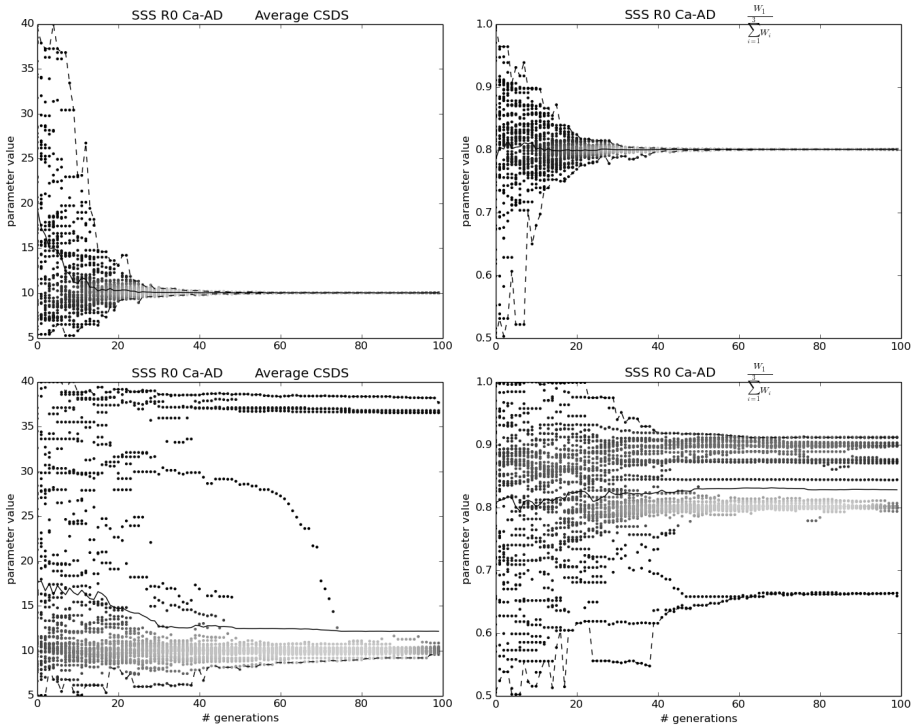

Figure 5. Parameter evolution plots for the low-charge smectite in assemblage 3. Plots for the multi-specimen setup are in the top row, for the AD single pattern setup in the bottom row. Legend as in Fig. 3.

GMDD
8, 2497–2528, 2015
PyXRD v0.6.2
M. Dumon and E. Van Ranst

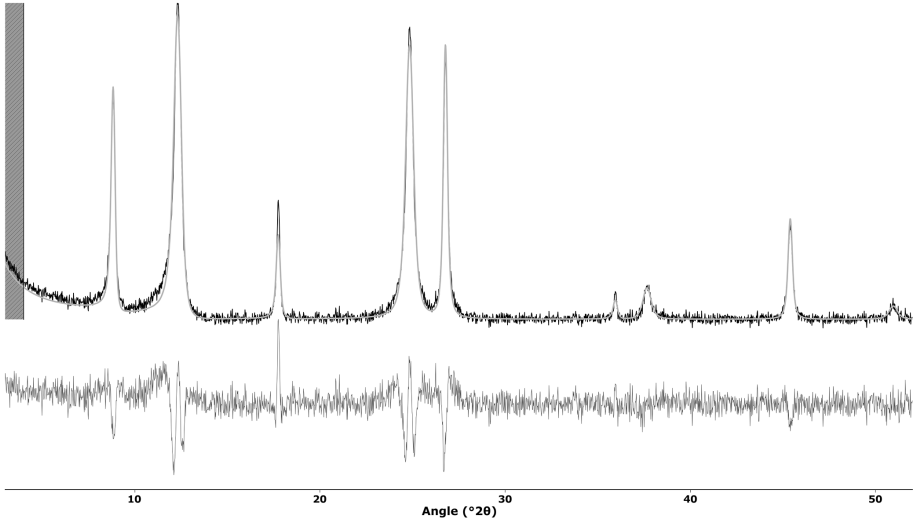

Figure 6. The input (black solid line) and refined (grey solid line) AD pattern and their difference (grey solid line at the bottom) for the multi-specimen setup of assemblage 4. An observant user should see the mismatches in the patterns and realize his model needs improvement.

GMDD
8, 2497–2528, 2015

PyXRD v0.6.2

M. Dumon and
E. Van Ranst